AIAA JOURNAL
Vol. 40, No. 6, June 2002

Filtered Thomson Scattering in an Argon Plasma

Sohail H. Zaidi* and Z. Tang†
Princeton University, Princeton, New Jersey 08540
A. P. Yalin‡
Stanford University, Stanford, California 94305-3032
P. Barker§
Heriot–Watt University, Edinburgh, Scotland EH14 4AS, United Kingdom
and
R. B. Miles¶
Princeton University, Princeton, New Jersey 08540

A filtered Thomson scattering technique has been developed to measure electron temperature T_e and electron number density n_e in an atmospheric pressure argon plasma. The problems of the strong background scattered light and the high plasma luminosity were resolved by employing an atomic vapor filter that provided strong attenuation of stray scattered light at the laser wavelength while simultaneously allowing the passage of the spectrally broad Thomson scattered light. A relatively low-power Ti: sapphire laser (about 50 mJ/pulse) was used in conjunction with an optically thick rubidium notch filer. High spectral purity of the laser was achieved by developing an amplified stimulated emission filter. Because of the geometrical constraints of the plasma arc source, experiments were performed in the backscatter geometry. Information on the electron number density and the electron temperature was derived from the Thomson signal by fitting a model curve to the data. The measurement results gave an electron temperature of 0.82 ± 0.06 eV and electron number density of $1.61 \times 10^{16} \pm 0.05 \times 10^{16}$ electrons/cm^3.

Introduction

PLASMA diagnostics have gained considerable attention in recent years due to their vast industrial applications.[1] Particularly, these diagnostics are in high demand in plasma aerodynamics where both intrusive and nonintrusive techniques are used to conduct plasma studies. The research work conducted in the former Soviet Union in 1990s indicated that the vehicle aerodynamics, particularly the shock wave, may be altered by the presence of a plasma.[2] Since then, several theoretical and experimental studies have been conducted to investigate the mechanisms of plasma effects on supersonic flows, especially on shock waves.[3–5] The mechanisms involved are complicated, and a complete understanding of the impact of plasma in such environment needs a thorough understanding of the plasma characteristics. In general, measurements of electron temperature T_e, electron number density n_e, ion temperature T_i, and ion number density n_i are required for the effective control of plasma. Various intrusive and nonintrusive methods have been extensively used to make these measurements within plasmas.

Langmuir probes are widely recognized as a standard tool to measure the local average of n_e and T_e in low-temperature and weakly ionized plasmas that are usually encountered in the semiconductor, optics, and polymer industries.[6] In general these probes are limited to the edge region of the plasmas because they can be damaged by the intense heat flux at the central region of the plasmas. As reported in Refs. 1 and 7, langmuir probes can be used no more than 1–2 cm inside the plasmas of small Tokamaks, 1–2 cm outside the limiter in large Tokamaks, and just 0.1– 0.5 cm inside the separatrix in heated diverted plasmas. Langmuir probe techniques have been recently refined[7] to examine edge fluctuation phenomena in Tokamak plasmas. In spite of their usefulness, the intrusive nature and their restricted application to the low-temperature plasmas make these probes unsuitable for high-temperature plasma studies.

Among the nonintrusive techniques that have been used to investigate plasmas, Thomson scattering has emerged as a powerful tool for plasma characterization.[8–11] This nonintrusive technique has been found to be well suited to the confined plasmas, where geometrical constraints put restrictions on the use of conventional techniques. Because of its extensive use, several Thomson scattering systems have emerged that have been designed by various research groups to suit their plasma conditions and geometry. Issues related to system alignment, calibration and optical access have been addressed in a rigorous manner.[12–15] Experiments in plasmas with electron densities in the range of $10^{17} < n_e < 10^{21}$ cm^{-3} and electron temperatures in the range of $1 < kT_e < 5$ eV are now being performed.[13,14] Recently attempts have been made to lower the detection limit for Thomson scattering measurements to below 10^{12} cm^{-3}. This density regime is commonly found in glow discharges that are used in industrial applications, including etching and deposition.

In spite of several advantages, including the nonintrusiveness of the technique, the high spatial and temporal resolution, and the ease in interpretation of data, Thomson scattering does have limitations. The Thomson scattering signal has to compete with plasma emission and the elastic background radiation, both of which can mask the Thomson signal. To minimize the uncertainties in the measured Thomson signal, it is of vital importance to eliminate the interference effects from stray light and the background radiation. To overcome the problems of stray light and the background radiation, an atomic dispersive resonance filter was developed. One prominent feature of the filter was to provide large spectral dispersion and resolution in the spectral region that was very close to the resonance line. The details of the Thomson scattering technique, the design and development of the filter, and the details on the successful detection of the Thomson signal from a plasma source are presented in the following sections.

Thomson Scattering

When a laser beam is passed through a plasma, the scattered light consists mainly of three components, namely, Thomson scattering,

Presented as Paper 2001-0415 at the AIAA 39th Aerospace Sciences Meeting, Reno, NV, 8–11 January 2001; received 12 March 2001; revision received 3 October 2001; accepted for publication 19 October 2001.

*Research Scientist, Department of Mechanical and Aerospace Engineering.
†Graduate Student, Department of Mechanical and Aerospace Engineering.
‡Postdoctoral Associate, Department of Chemistry, High Temperature Gas Dynamics Laboratory, Building 520.
§Lecturer, Department of Physics.
¶Professor, Department of Mechanical and Aerospace Engineering.

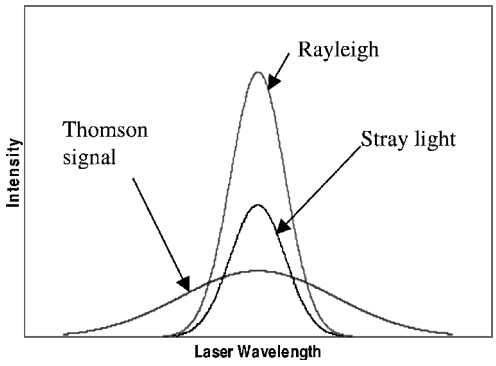

Fig. 1 Different components of the total scattered spectrum.

Rayleigh scattering, and elastic scattering (stray light component). The Thomson component arises from scattering from free electrons, whereas Rayleigh scattering arises from bound electrons. The stray light component comes from elastic scattering from various surfaces in the system and has the spectral shape of the laser. Figure 1 shows a simulated scattering spectrum. Note that both the Thomson and Rayleigh components are Doppler broadened but have very different spectral widths because of the much lower mass of electrons compared with that of atoms and ions. Figure 1 clearly indicates that an accurate Thomson signal can not be extracted without eliminating the Rayleigh and stray light components.

The line shape of the Thomson scattering profile is a complicated function of the parameter α, which, in turn, is a function of the scattering angle and the plasma characteristics (electron number density and electron temperature). The parameter α is defined as

$$\alpha = 1/k\lambda_D \approx \lambda_0/[4\pi\lambda_D \sin(\theta/2)] \tag{1}$$

where λ_D is the debye length in the plasma and k is the magnitude of the difference between the scattered wave vector $\boldsymbol{K}_S$ and the incident wave vector $\boldsymbol{K}_0$. Because the Thomson scattering is elastic, $|\boldsymbol{K}_S| = \boldsymbol{K}_0|$. The numerical value of the parameter α is given by the following relation:

$$\alpha = 1.58 \times 10^{-12}\lambda_0[n_e/T_e(1-\cos\theta)]^{\frac{1}{2}} \tag{2}$$

where λ is in angstrom, n_e in particles per cubic centimeter, and T_e in electron volts. Noted that the parameter α is a nondimensional number, and it represents the ratio of the period of the incident beam and scattering beam interference to debye length λ_D. If $\alpha \ll 1$, the scattering, comes from the uncorrelated electron motion and leads to incoherent Thomson scattering, whereas for $\alpha > 1$, collective electron motion plays a dominant role and leads to coherent Thomson scattering.

The factor governing the spectral profile of the Thomson scattering is referred to as the form factor and is denoted by $S(\boldsymbol{K}, \omega)$. The simplified expression for the form factor can be obtained by using the Salpeter's[15] approximations (see Ref. 8), which assume that, for most of the practical cases, the electron mass is much less than that of the ion and that the electron temperature and the ion temperature are comparable. Under this assumption, the form fact can be expressed as

$$S(\boldsymbol{k}, \omega) = S_e(\boldsymbol{k}, \omega) + S_i(\boldsymbol{k}, \omega) \tag{3}$$

$$S_e(\boldsymbol{K}, \omega) = \frac{1}{\sqrt{\pi}}\Gamma_\alpha(x_e)\,\mathrm{d}x_e$$

$$S_i(\boldsymbol{K}, \omega) = \frac{Z}{\sqrt{\pi}}\left[\frac{\alpha^2}{1+\alpha^2}\right]^2 \Gamma_\beta(x_i)\,\mathrm{d}x_i \tag{4}$$

$$\Gamma_{\gamma=\alpha,\beta}(x) = \frac{\exp(-x^2)}{\left[1+\gamma^2 R_\omega(x)\right]^2 + \left[\gamma^2 I_\omega(x)\right]^2} \tag{5}$$

where

$$\alpha = 1/K\lambda_D, \qquad \beta = Z(T_e/T_i)[\alpha^2/(1+\alpha^2)]$$
$$x_e = \omega/\sqrt{2}kv_e, \qquad x_i = \omega/\sqrt{2}kv_i$$
$$v_e = \sqrt{k_B T_e/m_e}, \qquad v_i = \sqrt{k_B T_i/m_i} \tag{6}$$

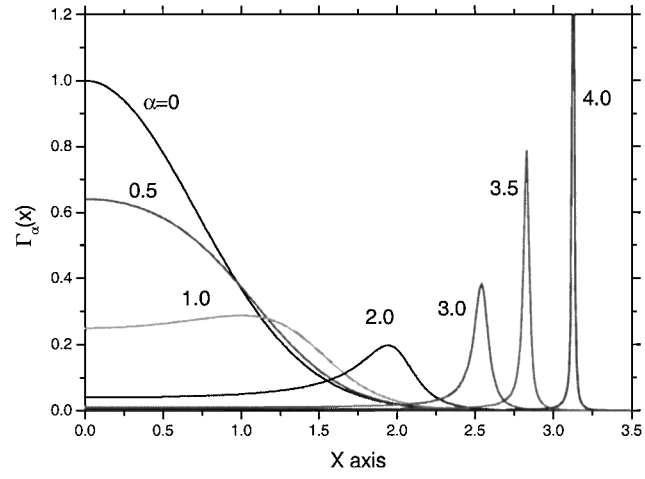

Fig. 2 Function $\Gamma_\alpha(x)$ vs x for various values of α (=0, 0.5, 1, 2, 3, 3.5, and 4).

T_e and T_i are the electron and ion temperatures, m_e and m_i are the electron and ion mass, respectively, and k_B is the Boltzmann constant. Both the nondimensional electron feature and the ion feature have the same spectral profile, determined by the $\Gamma_\gamma(x)$ function. However, the electron feature has much larger spectral spread, whereas the ion feature is much closer to the Rayleigh line. The function $\Gamma_\gamma(x)$ is even with respect to x and is shown in Fig. 2 for various values of α. The electron form factor has two symmetrically sharp resonance peaks around the incident light frequency, and the scattering at other frequencies can be neglected. This feature can be clearly seen in Fig. 2 for $\alpha = 4$.

The experimental detection of the line shapes provides information on plasma temperature, electron number, and ion number densities. Note that the frequency spectrum of the scattered light is strongly dependent on the scattering angle and the motion of the charged particles in the plasma. As compared to large scattering angles, spectral features at small scattering angles are compressed. In this regime, stray light is a major interference that must be rejected and attenuated for accurate measurement of the scattering profile. As explained earlier, the Thomson scattering signal is often very weak compared with the plasma emission intensities and Rayleigh scattering, and also the cross section for scattering of radiation from electrons is very small, which makes the scattered light extremely small as well. The following equation can be used to predict the number of photoelectrons N_{pe} in a scattering experiment[16]:

$$N_{\mathrm{pe}} = (I_L/h\nu)\Delta V n_e \sigma_{\mathrm{th}} \Delta\Omega \tau_L T \varepsilon \tag{7}$$

where I_L is the laser intensity, h Plank's constant, ν the laser frequency, ΔV the scattering volume, $\Delta\Omega$ the detection solid angle, τ_L the pulse length of the laser, T the transmission of the detection system, σ_{th} the Thomson scattering cross section, and ε the quantum efficiency of the detector used. For typical values of given parameters (laser power = 100 mJ/pulse, laser wavelength = 780 nm, beam diameter = 2 mm, $\tau_L = 10$ ns, $\Delta V = 6.3 \times 10^{-9}$, $T \sim 0.3$, $\varepsilon \sim 0.04$, $\Delta\Omega = 0.11$ srad, $\sigma_{\mathrm{th}} = 6.65 \times 10^{-29}$ m^2, and a plasma with electron density of $n_e = 10^{18}$ m^{-3}), Eq. (7) would result in about 21 photoelectrons detected per laser pulse. This is a very small signal, which, in the presence of a strong background emission from the plasma, can not be detected that easily. In most of the previous studies, very high-power pulsed lasers have been used to detect Thomson signals in various experimental facilities. A few such examples are presented in Table 1 (see Refs. 12 and 17–20).

Atomic Vapor Filters and Thomson Measurements

Atomic vapor filters have been widely used to suppress Rayleigh signals and the background noise that arises from the elastic scattering from medium particles and surfaces. Sabbaghzadeh et al.[21] were the first to use a resonant atomic vapor filter and succeeded to suppress the Rayleigh line by more than four orders of magnitude. Later, similar work by various researchers[22,23] confirmed that the filter technique can measure the Raman intensities of gases only

Table 1 Various examples of measuring Thomson signal using high-power lasers

Plasma source	Laser power	Detection	n_e, cm^{-3}	T_e	Reference
Alcator C-Model, Tokamak type, toroidal	Nd:Yag, 1.6 J/pulse	Avalanche photodiode	10^{13}–3×10^{15}	1–500 eV	12
Divertor of ITER (International Thermonuclear Experimental Reactor)	Nd:Yag, 1 J/pulse	Avalanche photodiode	10^{12}–5×10^{14}	5–500 eV	17
Divertor plasma	Nd:Yag, 1 J/pulse	Charge-coupled device (CCD) camera	0.05–8×10^{14}	1–500 eV	18
Tokamak plasma	Ruby laser, 12.5 J	Intensified CCD camera	10^{14}	100 eV–7 keV	19
RFX (Reverse Field Experiment) reverse, pinch field facility	Ruby laser, 15 J	MCP, PMT	5×10^{13}	50–2500 eV	20

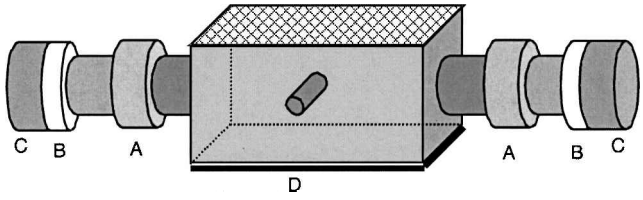

Fig. 3 Schematic diagram of the rubidium filter: A, B, and C represent 114-mm-diam joining flange, and cell D has the dimension of 254 × 127 × 127 mm.

a few gigahertz away from the Rayleigh line without any appreciable loss of Raman intensities. Based on the absorption atomic vapor filters, a recent work from Princeton University shows that neutral gas temperatures can be measured from the spectral profiles of the scattered light in a weakly ionized plasma at low-pressure (60 torr)(www.princeton.edu/~milesgrp). Such measurements have become possible due to the extremely high light rejection (1:10^{15}) provided by an absorption atomic vapor filter. The blocking line width of the filter is determined by the Doppler width of the transition and the length of the cell.

Because of their distinctive features, atomic vapor filters find very useful application in Thomson scattering measurements where the detection of the Thomson signal requires a strong suppression of the Rayleigh scattering and the elastic background resulting from medium particles and surfaces. Bakker and Kroesen[24] used a sodium vapor absorption cell along with a dye laser at 589 nm for Thomson measurements in a low-pressure discharge. The stray light was absorbed by the cell because it was resonant to the D_2 transition of sodium. The experimental setup to detect the Thomson signal was calibrated by the Raman scattering spectrum that was obtained from nitrogen. The Thomson scattering experiment was performed in a neon/mercury fluorescent lamp. With the experimental arrangement described in Ref. 24, Bakker and Kroesen were able to detect the Thomson signal from which the information on the electron temperature (0.9 eV) and the electron number density (1.3×10^{12} cm^{-3}) was extracted.

In the present work, we developed a rubidium notch filter in which rubidium D_2 line was used to suppress the elastic stray light to detect Thomson scattering for an atmospheric pressure argon arc plasma. Figure 3 shows the physical dimensions of the filter used in this work. A Ti:sapphire laser system (explained in the next section) was used at 780 nm so that the stray light and the Rayleigh scattering became resonant to the D_2 transition of rubidium. Table 2 shows the main differences between the experiment performed by Bakker and Kroesen[24] and the current work presented in this paper.

Before employing this filter in the Thomson experiment, the performance of the filter was thoroughly investigated. Various experiments were performed to obtain the absorption profiles at various operating conditions. Figure 4 shows both the theoretical and experimental results for the absorption profiles of the filter at various temperature gradients. As the density gradient increases across the filter, the absolute number density also increases, and the filter becomes more optically thick, a feature clearly seen in Fig. 4. During this experiment, the windows temperature was kept constant at 180°C so that the rubidium vapor condensed out along the filter arms before they could reach the windows. Figure 4 shows a good agreement between the theoretical predictions and the experimental data obtained for various cases. The performance of the filter was also confirmed by obtaining one-dimensional spectroscopic profile of the

Table 2 Comparison between current work and that performed by Bakker and Kroesen[24]

Parameter	Ref. 24	Present
Laser source	Dye laser	Ti:sapphire laser
Laser wavelength, nm	589	780
Laser power, mJ/pulse	60	50
Pulse width, ns	30	10
Laser ASE	10^{-4}	10^{-2}
Plasma source	Ne/Hg fluorescent lamp 10 mbar neon/2 Pa mercury	Argon maxiarc source
ASE filter	20-fold prism monochromator	20-fold prism monochromator
Detection angle	90 deg	Backscatter geometry
Measured electron temperature, eV	0.9	0.82
Measured electron number density, cm^{-3}	10^{12}	10^{16}

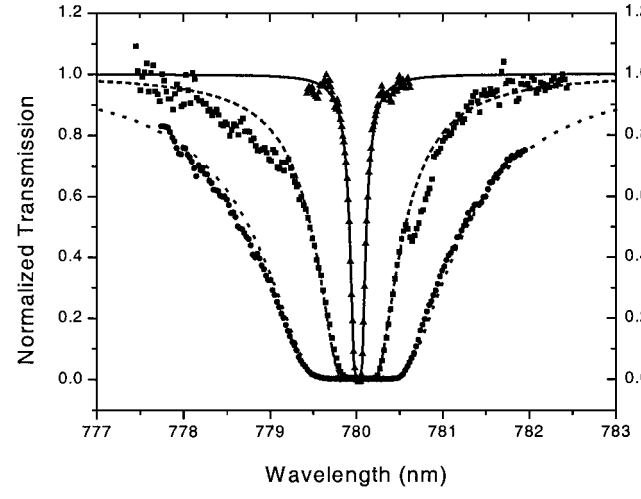

Fig. 4 Transmission profiles with measured and model predictions: ●, ■, and ▲ represent data taken for a temperature gradient of 287–60°C, 258–60°C, and 208–60°C, respectively.

rotational Raman scattering from CO_2. The filter was heated from below while keeping the top at a lower temperature, thereby creating a density gradient in the filter that was used to disperse the spectrum. Figure 5 shows the CO_2 rotational Raman spectrum. In this work a monochromator (McPherson Model 303; grating 1200 g/mm and exit slit 150 μm) was used to disperse the Raman rotational lines. Figure 5 shows the average intensity after the slit exit as a function of the slit spatial location. It is clear that the first several rotational lines experienced a large deviation. Figure 5 also gives the theoretical predictions for the rotational lines and their relative strengths. Further details of this work have been included in Ref. 23. Note that for the current study the rubidium filter was not used as a dispersive element but was only incorporated as a notch filter to suppress the elastic stray light.

Laser System

An existing Ti:Al_2O_3 laser was modified for this work.[25] This custom-built Ti:sapphire laser system is injected, seeded, and operated with a novel cavity-locking scheme, which ensures almost transform-limited narrow-linewidth single-mode output. The seed

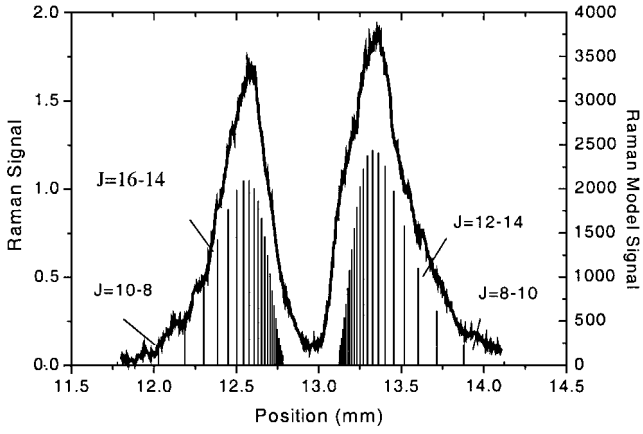

Fig. 5 One-dimensional carbon dioxide rotational Raman spectroscopic profile. (Vertical axes have arbitrary units.)

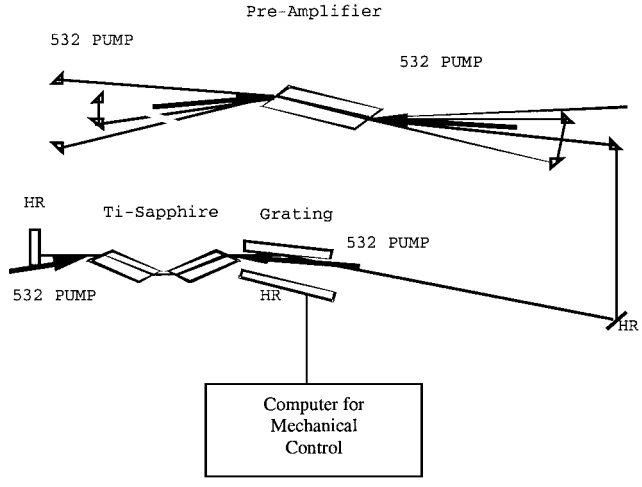

Fig. 6 Schematic layout for the computer-controlled, narrow-linewidth Ti:sapphire laser system.

source, a continuously tunable, continuous-wave Ti:sapphire laser, is tuned by modifying its effective cavity length and is stabilized via feedback through an intracavity etalon. The pulsed Ti:sapphire resonator is pumped by a frequency-doubled Nd:YLF laser. Figure 6 is a schematic diagram for the injection-seeded, cavity-locked Ti:sapphire system employed in this work. Thomson scattering is frequency independent, and thus, the fundamental wavelength of the tunable Ti:Al_2O_3 was used in this study. In the fundamental mode, this laser runs at 10 Hz and yields as much as 50 mJ of energy per pulse in the infrared region (about 780 nm).

Plasma Source

To demonstrate filtered coherent Thomson scattering, a stable uniform plasma source with high electron number density was required. An argon maxiarc source was obtained from National Institute of Standards and Technology (NIST), Optical Technology Division. Figure 7 shows a diagram of the argon arc system. This well-characterized arc source is constructed essentially of five stainless steel plates separated by insulating rings and clamped together to form the device. All five plates are water cooled. A flow rate of at least 6 l/min of water is needed for proper cooling. Argon gas was chosen as the operating gas (5000 cm^3/min) because of its suitability in providing a stable discharge. The discharge is initiated by applying a voltage between the electrodes and then inserting a tungsten rod, which is externally connected to the anode, until it touches the cathode protruding into the arc channel. The arc was constrained in the middle narrow channel (2.0-mm diam and 10 mm long) of the device. This has been measured to be in thermodynamic equilibrium with an electron number density of about 10^{17} cm^{-3} corresponding to a temperature of about 1 eV (private correspondence with NIST). Further details on argon arc source may be found in Ref. 26.

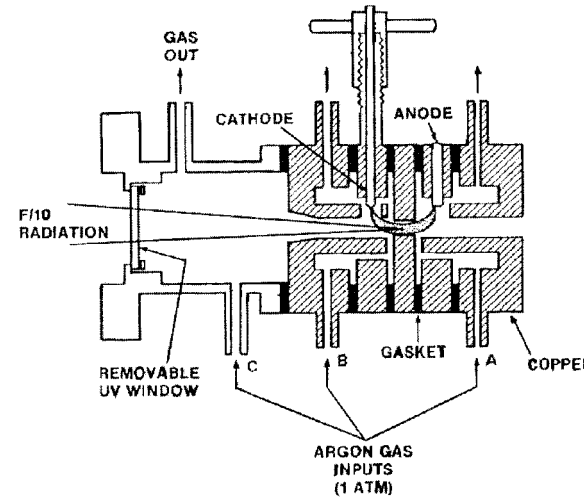

Fig. 7 Diagram of the argon arc system.

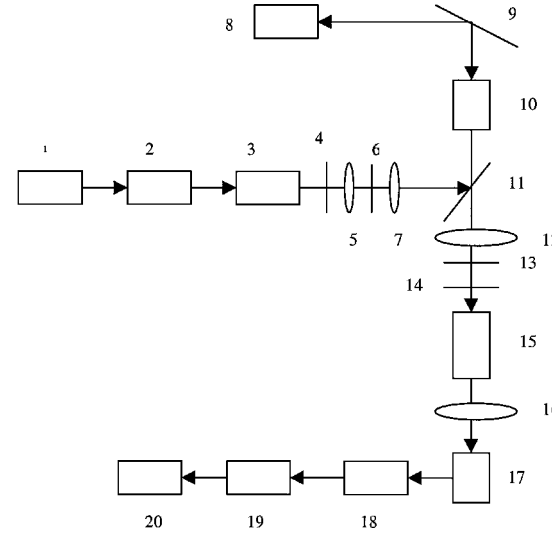

Fig. 8 Backscatter experimental setup for Thomson scattering. Components: 1, Ti:sapphire laser; 2, pulse Ti:sapphire laser; 3, ASE filter; 4, 6, and 13, iris; 5, 7, 12, and 16, lenses; 9 and 11, mirror; 10, argon arc plasma; 15, rubidium filter; 17, spectrometer; 18, photomultiplier tube; 19, boxcar; 20, computer; and 8, laser dump.

Plasma Luminosity and Amplified Stimulated Emission

Note that, due to geometrical constraints, the arc lamp employed in this study can only be used to detect the Thomson features in the backward or forward directions. Recall that the line shape of the scattered light spectrum is a strong function of the scattering angle, parameter α, electron number density, and electron temperature. In this work, where electron number density approximately equals 10^{16} cm^{-3} and electron temperature T_e is about 1 eV, the backward Thomson profiles approximates a Gaussian shape. In forward scattering, two distinctive peaks appear about the central peak, which represents the ion contributions overlapped by the Rayleigh peak.

The experiment was set up to detect the Thomson features around the laser line (780 nm) in the backscatter geometry. Figure 8 shows the general experimental setup employed in this study. The first experiment was performed without component 3 [amplified stimulated emission (ASE) filter] shown in Fig. 8. The atomic filter was heated up to 410°C, and appropriate spatial filters were used to eliminate the background elastic scattering. Because the Thomson signal will be polarized in the plane of the incident laser, a polarizer was used to further reduce the interference from the stray light and plasma luminosity. The laser was tuned on the resonance with the rubidium D_2 line. Although the Rayleigh and background elastic scattering was greatly attenuated through the filter, we were

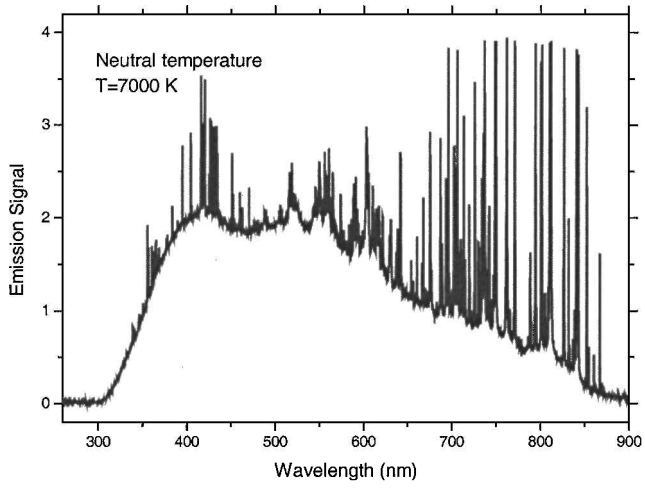

Fig. 9 Experimentally measured spectral profile of the argon arc lamp. (Vertical axes have arbitrary units.)

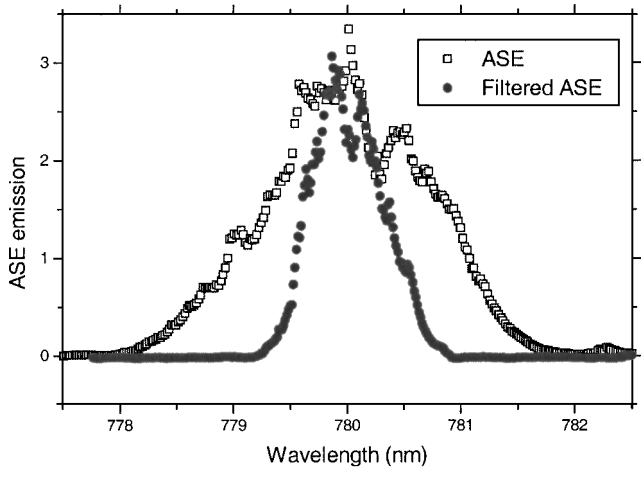

Fig. 10 Experimentally measured ASE emission with and without the ASE filter. (Vertical axes have arbitrary units.)

unable to detect any Thomson signal. Further careful investigation revealed two main problems. The first was the luminosity of the plasma source, and the second was the amplified stimulated emission from the laser itself. Both of these factors played a vital role in masking the Thomson signal. The spectral profile of the plasma source was investigated by collecting the emission from the source into a monochromator. Figure 9 shows a typical scan. The entrance and the exit slits of the monochromator (McPherson Model 303; grating 1200 g/mm) were fixed at 120.0 and 100.0 μm, respectively. The emission profile is significantly attenuated in the ultraviolet region. This was because of the collecting lens, which was made of Pyrex®. When the arc emission is assumed to be quasi-blackbody radiation, the emission peak around 400 nm, using the Wein's displacement law ($\lambda_{\mathrm{pm}} T = 2.8978 \times 10^{-3}$), gives a thermal temperature of the arc around 7000 K. Figure 9 also shows that the plasma emission background in the infrared is significantly lower than that in the visible region, but even this background was strong enough to mask the Thomson signal. To reduce the luminosity, the plasma source was operated at a lower current (about 20 A).

As mentioned earlier, the laser system used in this experiment was an injection-seeded laser that produces a narrow linewidth output at high energy. The disadvantage lies in that the amplifier not only amplifies the input field from the laser oscillator but also amplifies the spontaneous radiation, which resembles the unseeded laser emission. This radiation is ASE. The problems associated with ASE in Ti:sapphire systems have been discussed in detail in Refs. 27 and 28. To obtain a spectral scan of the ASE component of the injection-seeded Ti:sapphire laser used in this study, the center laser line (width ~100 MHz) was tuned to the rubidium D_2 resonance and was suppressed by the rubidium notch filter. Figure 10 shows that the

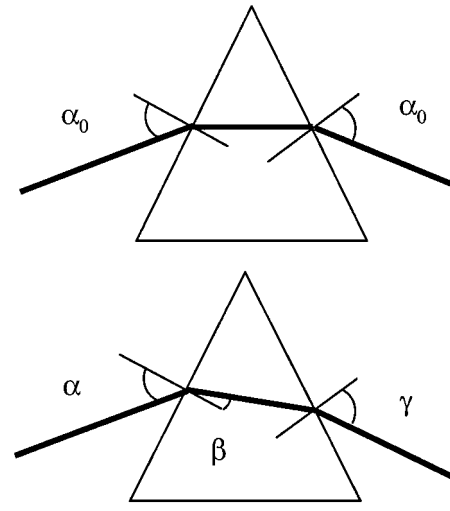

Fig. 11 Definition of various angles defined for the prisms in the ASE filter.

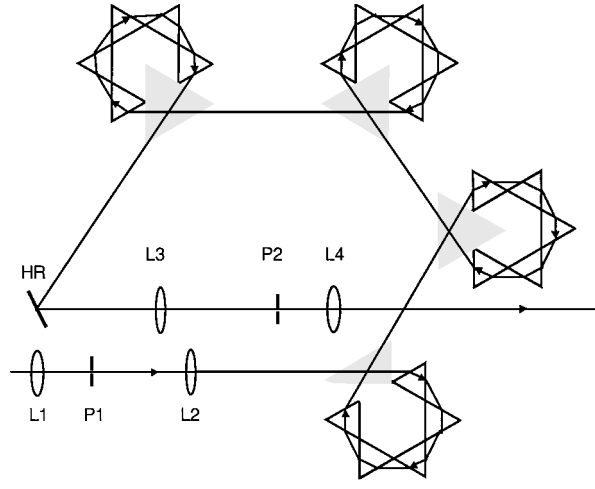

Fig. 12 ASE filter and the associated optical setup.

full width at half-maximum of the ASE component is about 2.0 nm, corresponding roughly to the unseeded spectral width. This high level of ASE lead to the unwanted fluorescence in the plasma and masked the required Thomson signal. To reduce the ASE level, an ASE filter based on the work of Bakker et al.[29] was reproduced. This filter was consisted of 20 prisms (SF10 glass), which were oriented in four groups. For an equilateral prism and for a symmetrical zero beam, α_0, as defined in Fig. 10, was calculated as 58.89 deg, which is slightly lower than the Brewster angle (59.71 deg). This difference caused slightly higher reflection losses. The Fresnel reflection loss per prism is 2.3×10^{-4}, whereas the internal transmission for 15-mm SF10 glass is 0.997. The deviation with respect to the zero beam for angle γ (as defined in Fig. 11) was found by the following relation:

$$\delta\gamma_{20} = 20\left[2\frac{\tan(\alpha_0)}{n_0}\left|\frac{\mathrm{d}n}{\mathrm{d}\lambda}\right|_0\right]\delta\lambda = 2\,\mathrm{mrad/nm} \qquad (8)$$

Figure 12 shows the way the ASE prism filter was incorporated in the experimental scheme. Spatial filters were used before and after the prism filters, and the incident beam was expanded to 10-mm-diam beam to avoid any damage on the glass prisms. The rejection of the light source occurs primarily at the exit pinhole due to the spatial spread of the ASE component on the focusing plane. Because of the high laser power, optical breakdown of air was observed at focusing spots. Optical breakdown is undesirable because it significantly reduced the laser power and also destroyed the Gaussian spatial profile. In the work, a purge gas (nitrogen) was used to eliminate this problem. Note that, because the incident angle on each of

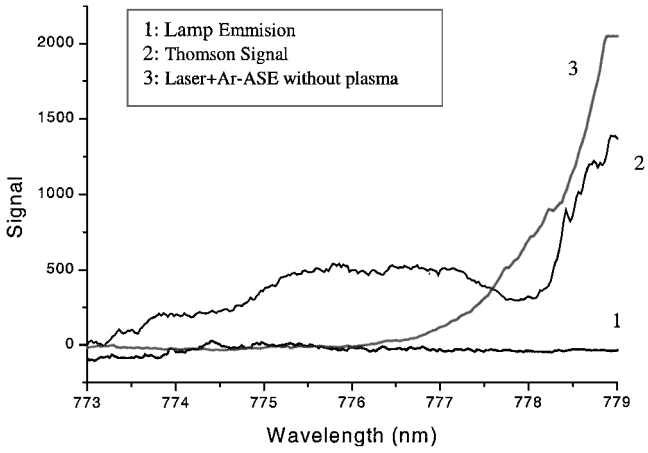

Fig. 13 Experimental results showing Thomson signal along with the lamp emission.

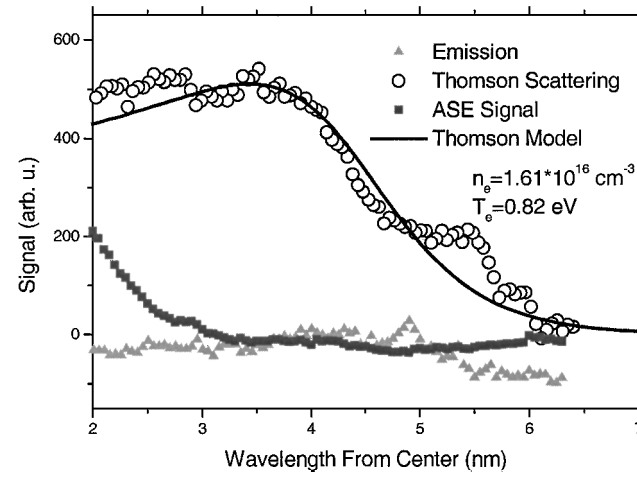

Fig. 14 Measured Thomson scattering spectrum, along with the spectrum of the plasma emission with the laser off and the laser ASE spectrum with the plasma off.

the prism surfaces was close to the Brewster angle, the total power loss observed through the ASE reduction filter assembly was less than 10%. This ASE filter, along with the atomic absorption filter, was used to suppress the strong elastic light and Rayleigh scattered light components (shown in Fig. 1), and the Thomson measurements were made, which will be explained in the next section.

Thomson Measurement

The experimental setup shown in Fig. 8 was used to detect the coherent Thomson features. The ASE filter shown in Fig. 12 has been marked as component 3 in Fig. 8. The atomic filter was heated up to 410°C and appropriate spatial filters were used to eliminate the background elastic scattering.

Before making any final measurements, various steps were taken to ensure the presence of the Thomson signal. The alignment of the scattering detection system was checked by observing the peak of Stokes Raman scattering of carbon dioxide gas. The laser frequency was locked at rubidium D_2 line, and the spectrometer was scanned across the laser line. After collecting the Thomson signal, the experiment was repeated without the plasma to detect any laser background. Similarly, a plasma scan without the laser was performed to ensure that plasma luminosity did not change abruptly in the spectral range where the Thomson signal was being collected. Results from these three experiments have been plotted in Fig. 13 clearly showing the presence of the Thomson profile from which the electron temperature and electron number density can be derived. Note that, in Fig. 13, the increased signal from 778 to 780 nm is due the strong elastic laser scattering and Rayleigh scattering. The rubidium absorption filter suppressed the radiation at laser line center of 780.02 nm while some portion of the laser ASE component passed through the filter causing the signal near the laser center wavelength to increase. For the Thomson scattering curve fit, the section of the profile not directly influenced by the Rayleigh line was used to obtain the electron temperature and electron number density. This was achieved by matching the experimental line profile with the theoretical model described in Ref. 15. In this study, only the electron component of the Thomson scattering was analyzed. The theoretical line shape depends on the T_e and n_e in a nonlinear way and is given by

$$S_e(\Delta\lambda) \propto \Gamma_\alpha \left\{ \Delta\lambda \Big/ \left[2\lambda_0 \sin(\theta/2) \sqrt{2k_B T_e / m_e c^2} \right] \right\} \qquad (9)$$

where λ_0 is the laser wavelength, $\Delta\lambda = \lambda - \lambda_0$ is the wavelength from the laser line, θ is the scattering angle, and c is the speed of light. The nonlinear fitting was performed using the Levenberg–Marquardt algorithm (see Refs. 30 and 31), and the fitted curve is shown in Fig. 14. The theoretical line shape was fitted to the data to give the electron number density and electron temperature. The argon current was 20 A and the discharge voltage was 47 V. The measurement results gave an electron temperature of 0.82 ± 0.06 eV and an electron number density of $1.61 \times 10^{16} \pm 0.05 \times 10^{16}$ electrons/cm^3. The uncertainty in the measurements was determined by the standard deviation of the nonlinear curve fit between the experimental data and the theoretical Thomson scattering line shape function. From the previous estimation for the neutral gas temperature, the arc is in thermal nonequilibrium with an electron temperature about 2500 K higher than the ion temperature.

Conclusions

Filtered coherent Thomson scattering technique has been used to detect the Thomson signal from an argon plasma. The Thomson measurements were taken in the infrared region, where the Rayleigh background from the neutrals was reduced as compared with Thomson scattering in the visible and in the UV region. In this study, an approach of rubidium notch filtered with a high spectral purity and narrow linewidth laser has been demonstrated to suppress the laser background and to capture backward Thomson scattering from the source. The information on the electron temperature and the electron number density was extracted from the Thomson signal by fitting a model curve to the data.

Acknowledgments

This work was supported by a Small Business Innovative Research project on filtered coherent Thomson scattering fort plasma diagnostics and under the auspices of the air plasma ramparts Multidisciplinary University Research Initiative program under Robert Barker. We thank James Taylor at the Princeton Plasma Physics Laboratory for the vacuum helium leak test for the filter cell. Michael Souza of the Princeton University Chemistry Department made the rubidium filling manifold. We thank Philip Howard for the mechanical design and the drawing for the cell. Iaonnis Kominis of the Princeton University Physics Department helped us to fill rubidium into the filter cell. Their generous help is greatly appreciated.

References

[1]Bretz, N., "Diagnostic Instrumentation for Microturbulence in Tokamaks," *Review of Scientific Instruments*, Vol. 68, No. 8, 1997, pp. 2927–2964.

[2]Kimmel, R., Orkwis, P., and Lurie, E., "Plasma Aerodynamics and Flow Control," *Aerospace America*, Vol. 37, No. 12, 1999, pp. 10, 11.

[3]Macheret, S. O., Ionikh, Y. Z., Martinelli, L., Barker, P. F., and Miles, R. B., "External Control of Plasmas for High-Speed Aerodynamics," AIAA Paper 99-4853, 1999.

[4]Miles, R. B., "Flow Control by Energy Addition into High-Speed Air," AIAA Paper 2000-2324, June 2000.

[5]Ionikh, Y. Z., Chernysheva, N. Y., Yalin, A. P., Macheret, S. O., Martinelli, L., and Miles, R. B., "Shock Wave Propagation Through Glow Discharge Plasmas: Evidence of Thermal Mechanism of Shock Dispersion," AIAA Paper 2000-0714, Jan. 2000.

[6]Batani, D., Alba, S., Lombardi, P., and Galassi, A., "Use of Langmuir Probes in a Weekly Ionized, Steady-State Plasma with Strong Magnetic Field," *Review of Scientific Instruments*, Vol. 68, No. 11, 1997, pp. 4043–4050.

[7]Allen, S. L., "Recent Results from Tokamak Divertor Plasma Measurements," *Review of Scientific Instruments*, Vol. 68, No. 2, 1997, pp. 1261–1267.

[8]Kunze, H. J., *Plasma Diagnostics*, edited by W. Lochte-Holtgreven, North-Holland, Amsterdam, 1968, pp. 550–565.

[9]Desilva, A. W., and Goldenbaum, G. C., "Plasma Diagnostics by Light Scattering," *Method of Experimental Physics*, edited by H. R. Griem and R. Lovberg, Academic Press, New York, 1970, pp. 61–111.

[10]Bray, B., Hsieh, C., Carlstrom, T. N., and Makariou, C. C., "Upgraded Calibrations of the Thomson Systems at DIII-D," 13th Topical Conf. on High Temperature Plasma Diagnostics, June 2000.

[11]Sheffield, J., *Plasma Scattering of Electromagnetic Radiation*, Academic Press, New York, 1975, pp. 1–22.

[12]Dimock, D., Grek, B., Johnson, D., LaBombard, B., Lipschultz, B., and McCracken, G., "A Compact Thomson Scattering System," *Review of Scientific Instruments*, Vol. 68, No. 1, 1997, pp. 700–703.

[13]Smith, O. R. P., Gowers, C., Nielsen, P., and Salzmann, H., "A Self-Calibration Technique for a Thomson Scattering System," *Review of Scientific Instruments*, Vol. 68, No. 1, 1997, pp. 725–727.

[14]Barth, C. J., Beurskens, M. N. A., Chu, C. C., Donne, A. J. H., Cardozo, N. J. L., Herranz, J., Meiden, H. J. V. D., and Pijper, F. J., "A High Resolution Multiposition Thomson Scattering System for the Rijnhuizen Tokamak Project," *Review of Scientific Instruments*, Vol. 68, No. 9, 1997, pp. 3380–3392.

[15]Salpeter, E. E., "Electron Density Fluctuations in a Plasma," *Physical Review*, Vol. 120, No. 5, 1960, pp. 1528–1535.

[16]Muraoka, K., Uchino, K., and Bowden, M. D., "Diagnostics of Low-Density Glow Discharge Plasmas Using Thomson Scattering," *Plasma Physics Control Fusion*, Vol. 40, 1998, pp. 1221–1239.

[17]Carlstrom, T. N., Hsieh, C. L., Stockdale, R., Nilson, D. G., and Hill, D. N., "Initial Operation of the Divertor Thomson Scattering Diagnostic on DIII-D," *Review of Scientific Instruments*, Vol. 68, No. 2, 1997, pp. 1195–1200.

[18]Nilson, D. G., Hill, D. N., Evans, J. C., Carlstrom, T. N., Hsieh, C. L., and Stockdale, R., "Thomson Scattering Stray Light Reduction Technique Using a CCD Camera," *Review of Scientific Instruments*, Vol. 68, No. 1, 1997, pp. 704–707.

[19]Beursken, M. N. A., Barth, C. J., Chu, C. C., Donne, J. H., Cardozo Lopes, N. J., Van der Meiden, H. J., and Pijper, F. J., "Double Pulse Thomson Scattering System at RTP," *Review of Scientific Instruments*, Vol. 68, No. 1, 1997, pp. 721–724.

[20]Bassan, M., Pasqualotto, R., Sardella, A., and Giudicotti, L., "Development of a Multipoint Thomson Scattering for a Large Reverse Field Pinch Experiment," *Review of Scientific Instruments*, Vol. 61, No. 10, 1990, pp. 2846–2848.

[21]Sabbaghzadeh, J., Buell, W., Holder, J., and Fink, M., *Applied Physics B*, Vol. 60, 1995, pp. S261–S265.

[22]Finkelstein, N. D., Yalin, A. P., Lempert, W. R., and Miles, R. B., "Dispersion Filter for Spectral and Spatial Resolution of Pure Rotational Raman Scattering," *Optics Letters*, Vol. 23, No. 20, 1998, pp. 1615–1617.

[23]Tang, Z., Zaidi, S. H., and Miles, R. B., "Density Gradient Rubidium Dispersive Absorption Filter for Low Wave Number Raman and Thomson Scattering," AIAA Paper 2000-0644, Jan. 2000.

[24]Bakker, L. P., and Kroesen, G. M. W., "Thomson Scattering Using an Atomic Notch Filter," *Review of Scientific Instruments*, Vol. 71, No. 5, 2000, pp. 2007–2014.

[25]Finkelstein, N. D., "An Ultraviolet Laser Source and Spectral Imaging Filters for Non Intrusive Laser Based Diagnostics," Ph.D. Dissertation, Dept. of Mechanical and Aerospace Engineering, Princeton Univ., Princeton, NJ, Jan. 1998.

[26]Bridges, J. M., and Ott, W. R., "Vacuum Ultraviolet Radiometry—The Argon Min-Arc as a New Secondary Standard of Spectral Radiance," *Applied Optics*, Vol. 16, No. 2, 1977, pp. 367–376.

[27]Barnes, N. P., and Barnes, J. C., "Injection Seeding I: Theory," *IEEE Journal of Quantum Electronics*, Vol. 29, No. 10, 1993, pp. 2670–2683.

[28]Barnes, N. P., and Barnes, J. C., "Injection Seeding II: Ti : AL_2O_3 Experiments," *IEEE Journal Quantum Electronics*, Vol. 29, No. 10, 1993, pp. 2684–2692.

[29]Bakker, L. P., Freriks, J. M., and Kroesen, G. M. W., "A New ASE Filter: The 20-Fold Prism Monochromator," *Rapid Communication, Measurement Science Technology*, Vol. 10, 1999, pp. L25–L28.

[30]Press, W. H., Teukolsky, S. A., Vetterling, W. T., and Flannery, B. P., *Numerical Recipes in Fortran: The Art of Scientific Computing*, Vol. 1, 2nd ed., Cambridge Univ. Press, Cambridge, England, U.K., 1986, pp. 675–683.

[31]Zhen, T., "Infra-Red Rubidium Atomic Resonant Filters for Low Wave Number Scattering," Ph.D. Dissertation, No. 3083, Applied Physics Group, Dept. of Mechanical and Aerospace Engineering, Princeton Univ., Princeton, NJ, Jan. 2001.

W. R. Lempert
Guest Associate Editor